AGU PUBLICATIONS

JGR

Journal of Geophysical Research: Atmospheres

RESEARCH ARTICLE
10.1002/2017JD027657

**Key Points:**
- Meteoric smoke in the mesosphere can be composed of magnetite, wüstite, magnesiowüstite, or iron-rich olivine
- Smoke compositions of pure pyroxene, hematite, iron-poor olivine, magnesium silicate, and silica are excluded
- Global meteoric influx estimates are 3.3 t $d^{-1}$ for ablated material only and 30 t $d^{-1}$ for the total influx

**Correspondence to:**
M. E. Hervig,
m.e.hervig@gats-inc.com

**Citation:**
Hervig, M. E., Brooke, J. S. A., Feng, W., Bardeen, C. G., & Plane, J. M. C. (2017). Constraints on meteoric smoke composition and meteoric influx using SOFIE observations with models. *Journal of Geophysical Research: Atmospheres*, *122*, 13,495–13,505. https://doi.org/10.1002/2017JD027657

Received 24 AUG 2017
Accepted 4 DEC 2017
Accepted article online 11 DEC 2017
Published online 22 DEC 2017



# Constraints on Meteoric Smoke Composition and Meteoric Influx Using SOFIE Observations With Models

**Mark E. Hervig[1], James S. A. Brooke[2], Wuhu Feng[2,3], Charles G. Bardeen[4], and John M. C. Plane[2]**

[1]GATS, Driggs, ID, USA, [2]School of Chemistry, University of Leeds, Leeds, UK, [3]NCAS School of Earth and Environment, University of Leeds, Leeds, UK, [4]National Center for Atmospheric Research, Boulder, CO, USA

**Abstract** The composition of meteoric smoke particles in the mesosphere is constrained using measurements from the Solar Occultation For Ice Experiment (SOFIE) in conjunction with models. Comparing the multiwavelength observations with models suggests smoke compositions of magnetite, wüstite, magnesiowüstite, or iron-rich olivine. Smoke compositions of pure pyroxene, hematite, iron-poor olivine, magnesium silicate, and silica are excluded, although this may be because these materials have weak signatures at the SOFIE wavelengths. Information concerning smoke composition allows the SOFIE extinction measurements to be converted to smoke volume density. Comparing the observed volume density with model results for varying meteoric influx (MI) provides constraints on the ablated fraction of incoming meteoric material. The results indicate a global ablated MI of 3.3 ± 1.9 t $d^{-1}$, which represents only iron, magnesium, and possibly silica, given the smoke compositions indicated here. Considering the optics and iron content of individual smoke compositions gives an ablated Fe influx of 1.8 ± 0.9 t $d^{-1}$. Finally, the global total meteoric influx (ablated plus surviving) is estimated to be 30 ± 18 t $d^{-1}$, when considering the present results and a recent description of the speciation of meteoric material.

## 1. Introduction

Meteoric smoke particles (MSP) result from the condensation of meteoroid ablation products and reside in the stratosphere and mesosphere (Plane, 2012). The present study uses observations from the Solar Occultation For Ice Experiment (SOFIE) at three wavelengths to constrain the composition of smoke particles in the mesosphere. Smoke composition is important for ion and neutral chemistry in the mesosphere and upper stratosphere (Frankland et al., 2015; James et al., 2017; Summers & Siskind, 1999), is relevant to the nucleation of polar mesospheric clouds (PMCs) (Havnes & Næsheim, 2007) and stratospheric aerosols, and is germane to astronomy. In addition, the interpretation of smoke observations will benefit from knowledge of smoke composition. For example, rocket in situ smoke observations require knowledge of smoke composition to correctly interpret the signals measured from charged particles (e.g., Hedin et al., 2007; Rapp et al., 2012).

The current understanding of MSP composition comes from a variety of atmospheric and laboratory measurements, but none of these were conducted on MSPs that were freely suspended in the middle atmosphere. Laboratory experiments suggest that smoke may consist of hematite ($Fe_2O_3$), goethite (FeOOH), fayalite ($Fe_2SiO_4$), silica ($SiO_2$), or olivine ($Mg_{2x}Fe_{2-2x}SiO_4$, $0 \leq \times \leq 1$) (Saunders & Plane, 2006, 2011). Measured optical signatures have suggested that meteoric remnants in the middle atmosphere (but not smoke) were composed of olivine (Klekociuk et al., 2005) and hematite (Bohren & Olivero, 1984). Observational evidence concerning smoke composition came from SOFIE observations, which indicated that the ice particles in PMCs contain a small amount of meteoric smoke ($\lesssim$3% by volume). The multiwavelength measurements were consistent with smoke composed of either carbon or magnesiowüstite ($Mg_xFe_{1-x}O$, $x$ = 0–0.6) (Hervig et al., 2012). Murphy et al. (1998) analyzed MSPs contained within stratospheric sulfate aerosols (SSA) and found Mg/Fe ratios that were consistent with extraterrestrial material. Carbon is not often considered as a candidate for MSP composition, although it can be present in meteoric material. Rotundi and Rietmeijer (2008) indicated that C could evaporate at meteoroid ablation temperatures and suggested that vaporized carbon might condense to form aerosols in the atmosphere. The more likely scenario, however, is that atomic C combines with oxygen to form CO and eventually $CO_2$. The present study offers the first observational constraints on MSP composition, from MSPs that were freely suspended in the middle atmosphere.

Estimates of the meteoric influx (MI) into Earth's atmosphere range from 5 to 270 t $d^{-1}$ (Gardner et al., 2014; Plane, 2012). Radar measurements show a ~30% seasonal increase in MI during autumn at high latitudes, but little or no seasonal variation at low latitudes (Janches et al., 2004; Marsh et al., 2013; Singer et al., 2004). Modeling studies show that the seasonal influx variation is largely absent in smoke, because transport is by far the dominant process behind smoke variability in the mesosphere and stratosphere (e.g., Megner et al., 2008). A recent investigation reports a total MI (TMI, ablated plus surviving material) of 43 ± 14 t $d^{-1}$ with around 80% of the meteoroids from Jupiter Family Comets, and the remainder from Halley Type/Oort Cloud comets and the asteroid belt (Carrillo-Sánchez et al., 2016). This daily influx was constrained by the vertical fluxes of Na and Fe atoms measured in the upper atmosphere, and the deposition of cosmic spherules at the surface. It was found that only ~18% of the incoming meteoric material is ablated (and is thus resident in the middle atmosphere), with the remainder falling quickly to the surface and possibly interacting to some extent with SSA. This ablated fraction is much lower than previous estimates, which suggested that more than 90% of the incoming material was vaporized during atmospheric entry (Taylor et al., 1998; Vondrak et al., 2008). Meteoric influx has implications for atmospheric chemistry, aerosol processes, ocean productivity, astronomy, and interpreting the accumulation of extraterrestrial material at the surface (Plane, 2012). Knowledge of smoke composition allows SOFIE extinctions to be converted into smoke volume densities ($V$, i.e., the volume of aerosol per unit volume of air). This in turn allows an estimate of the ablated MI through comparisons of the observations with modeled $V$ versus MI.

## 2. SOFIE Observations

SOFIE conducts solar occultation measurements from the Aeronomy of Ice in the Mesosphere (AIM) satellite, by monitoring the reduction in solar intensity as rays pass through the atmosphere on tangent paths during sunset or sunrise as viewed from the AIM satellite (Gordley et al., 2009; Russell III et al., 2009). SOFIE provides vertically resolved (~1.8 km) measurements and offers high sensitivity due to the bright solar source, long path length (~300 km), and a precise electro-optical system. Observations are taken continuously at latitudes from ~65° to 82°S (spacecraft sunset) and ~65° to 82°N (sunrise). Measurements at 16 wavelengths ($\lambda$ from 292 to 5,316 nm) are used to retrieve vertical profiles of temperature, PMC extinction, MSP extinction, and the abundance of five gaseous species ($O_3$, $H_2O$, $CO_2$, $CH_4$, and NO). Smoke extinction ($\beta(\lambda)$) measurements at 1,037 nm wavelength ($\lambda$) in the Southern Hemisphere (SH) were described by Hervig et al. (2009). The present study uses measurements at wavelengths of 330 and 867 nm, in addition to 1,037 nm. Observations at 330 nm have been available since November 2009, when the optics became sufficiently opaque within the ultraviolet to alleviate saturation of the 330 nm electronics (Hervig et al., 2012). It is possible that smoke is measured by some of the infrared aerosol measurements ($\lambda > 2{,}400$ nm). Such measurements will require additional efforts, for example, more accurate removal of gaseous interference, and interpretation of the infrared measurements is not attempted at this time. SOFIE currently offers smoke measurements in the SH only. The Northern Hemisphere measurements are from sunrises, which present unique signal calibration issues that are not yet resolved to a degree that allows reliable smoke retrievals (Hervig et al., 2009). The current SOFIE data are version 1.3, which is available online (sofie.gats-inc.com).

Because smoke extinction is extremely weak in the mesosphere, successful retrievals require averaging of the signals prior to retrieval. This approach is taken because the retrievals do not allow negative values and thus yield a high bias for measurements near the noise (see Hervig et al., 2009, for detail). The present study uses 5 day signal averages, as discussed in Hervig et al. (2017). Some additional enhancements to the retrievals were employed to reduce the smoke measurement uncertainties, as described now. In particular, errors in the 330 and 867 nm measurements can be significant and the smoke retrievals were often not successful in the middle mesosphere. The SOFIE signals contain a small amount of drift, which is due to heating of the system during solar view. This drift was found to be linear and is removed by extrapolating the drift characterized just above the atmosphere, down through atmospheric heights (Gordley et al., 2009). Note that the exo-atmospheric altitudes ($Z_0$) are defined as 110, 97, and 94 km, for the 330, 867, and 1,037 nm wavelength measurements, respectively, and that smoke extinctions are only retrieved below these heights. A closer examination of the SOFIE signals reveals that the drift corrections for the 330 and 867 nm measurements often contained errors that were on the order of the smoke signal. The present study therefore employed a modified approach where 5 day averages were constructed using the uncorrected signals, with the linear drift correction then performed on these average signal profiles. This approach was an improvement because

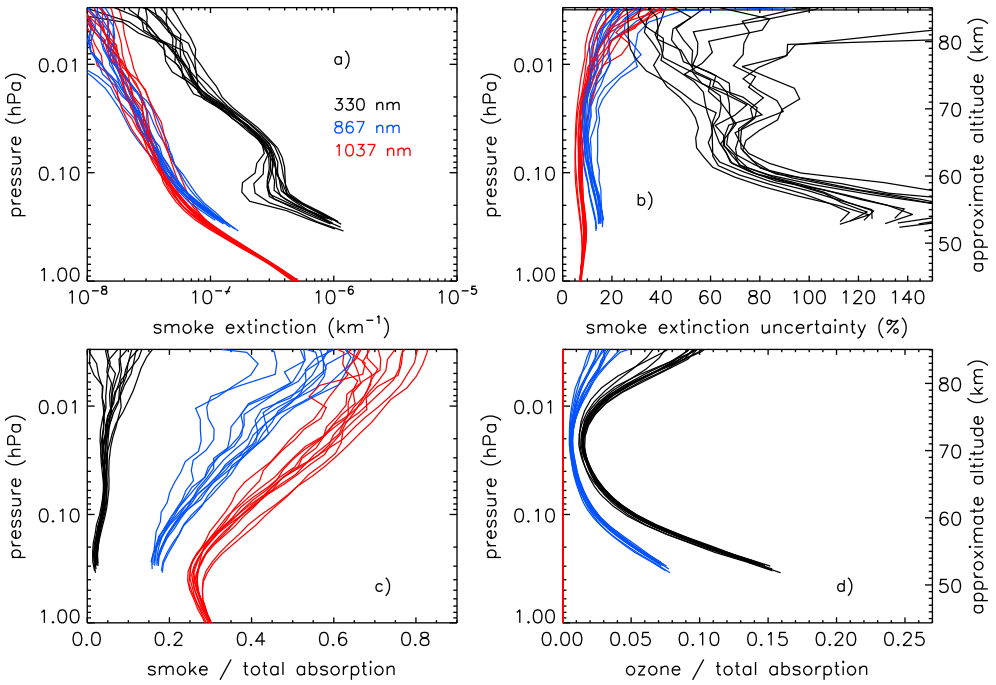


**Figure 1.** An example SOFIE results based on retrievals using 5 day signal averages, during April–May 2011 near ~70°S latitude. (a) Retrieved meteoric smoke extinction at three wavelengths as indicated by color. (b) Extinction uncertainty considering the measurement noise, signal correction errors, and errors in removal of Rayleigh and ozone interference, for three wavelengths. The fraction of total absorption due to (c) smoke and (d) ozone, for three wavelengths. Note that the remaining signal is due to Rayleigh scattering.

the signal drift is typically small and sometimes characterized by noise, which could result in a poor linear fit (and thus extrapolation) on individual events. Removing the average drift from the average signal reduced the statistical uncertainty in the drift corrections to levels that were below both the noise limit and the smoke signal. The retrievals used in this study also employed a spatial convolution of the field of view (FOV) and solar source, over the simulated signal profile. This is different from previous versions that subtracted the effects of FOV convolution from the measurements and accounted for solar refraction by modeling only the FOV center ray. While these approaches are easily sufficient for all other SOFIE retrievals, additional accuracy is needed when attempting to retrieve smoke extinctions, especially at 330 and 867 nm wavelengths. The most notable impact of the new algorithm was in the 330 and 867 nm extinction retrievals, which often failed above ~55 km altitude (in ~50% of events), but now routinely extend to ~85 km in the new version. This change is key to the present study that requires measurements at three wavelengths in the mesosphere to examine smoke composition. The 1,037 nm extinctions are generally from 10 to 40% higher within the mesosphere, compared to the previous version. At the time of this writing, these new retrievals were only available for 2011.

The uncertainty in measured smoke extinction is defined as the root-sum-square of the measurement noise, drift correction error, and errors in interference. Interference is due to $O_3$ and Rayleigh scattering at 330 and 867 nm, and only Rayleigh at 1,037 nm. The present study assumed 3% errors in total interference, which is consistent with an assessment of SOFIE density (proportional to Rayleigh) observations (Marshall et al., 2010) and $O_3$ errors (Gordley et al., 2009). The 330 nm smoke uncertainty is dominated by the Rayleigh (i.e., density) error for altitudes below ~85 km. The 867 and 1,037 nm smoke uncertainties are dominated by the noise above ~70 km, and Rayleigh errors below. Smoke extinction at 330 nm wavelength is ~5 to 10 times greater than at 867 or 1,037 nm (Figure 1a); however, it also has the largest uncertainty of the three wavelengths (Figure 1b). This occurs because smoke comprises less than 10% of the total 330 nm signal (Figure 1c), compared to 20–60% at the longer wavelengths. $O_3$ absorption accounts for roughly 2–20% (at ~70–45 km altitude) of the absorption at 330 and 867 nm wavelength and is negligible at 1,037 nm (Figure 1d). $O_3$ interference is removed using SOFIE retrievals of $O_3$ mixing ratio, which cover altitudes from ~53 to

**Table 1**
*Model Results for Various Smoke Compositions, and the Probability (Pb) That a Composition Was Observed Based on SOFIE-Model Comparisons*

| No. | Composition (name [a]/phase[b]) | $\beta(330)/\beta(1037)$[c] | $\beta(867)/\beta(1037)$[c] | $V/\beta(1037)$ ($\mu m^3\ cm^{-3}\ km$)[c] | Pb, this work (%)[d] | Pb, in PMCs (%)[e] | Fe influx ($t\ d^{-1}$)[f] |
|---|---|---|---|---|---|---|---|
| 1 | $Fe_3O_4$ (m/?) | 5.5 ± 1% | 0.98 ± 0% | $2.51 \times 10^2$ ± 0% | 40 | 14 | 0.8 |
| 2 | $Mg_{0.5}Fe_{0.5}O$ (Mw/c) | 5.4 ± 1% | 1.12 ± 0% | $3.93 \times 10^2$ ± 0% | 34 | 75 | 1.0 |
| 3 | $Mg_{0.3}Fe_{0.7}O$ (Mw/c) | 5.5 ± 1% | 1.18 ± 0% | $4.04 \times 10^2$ ± 0% | 37 | 82 | 1.2 |
| 4 | Fe (Iron/?) | 9.8 ± 1% | 1.39 ± 0% | $4.40 \times 10^2$ ± 1% | 43 | na[g] | 2.0 |
| 5 | $Mg_{0.2}Fe_{0.8}O$ (Mw/c) | 7.1 ± 1% | 1.20 ± 0% | $4.68 \times 10^2$ ± 0% | 75 | 81 | 1.5 |
| 6 | FeO (w/?) | 7.9 ± 1% | 1.23 ± 0% | $5.04 \times 10^2$ ± 0% | 71 | 82 | 1.8 |
| 7 | $Mg_{0.1}Fe_{0.9}O$ (Mw/c) | 8.2 ± 1% | 1.25 ± 0% | $5.45 \times 10^2$ ± 0% | 62 | 82 | 1.9 |
| 8 | $Mg_{0.6}Fe_{0.4}O$ (Mw/?) | 7.7 ± 1% | 1.13 ± 0% | $5.58 \times 10^2$ ± 0% | 75 | 65 | 1.2 |
| 9 | $Mg_{0.8}Fe_{1.2}SiO_4$ (o/g) | 8.0 ± 1% | 0.99 ± 0% | $1.51 \times 10^3$ ± 0% | 68 | 14 | 3.0 |
| 10 | $MgFeSiO_4$ (o/g) | 10.3 ± 1% | 1.04 ± 0% | $1.87 \times 10^3$ ± 0% | 34 | 13 | 3.6 |
| 11 | $Fe_2O_3$ (h/?) | 36.2 ± 1% | 1.51 ± 0% | $2.77 \times 10^3$ ± 0% | 0 | 39 | |
| 12 | $Mg_{0.4}Fe_{0.6}SiO_3$ (p/g) | 24.4 ± 1% | 1.25 ± 0% | $7.48 \times 10^3$ ± 0% | 0 | 3 | |
| 13 | $Mg_{0.5}Fe_{0.5}SiO_3$ (p/g) | 38.7 ± 1% | 1.37 ± 0% | $1.24 \times 10^4$ ± 0% | 0 | 3 | |
| 14 | $Mg_{0.6}Fe_{0.4}SiO_3$ (p/g) | 58.8 ± 1% | 1.41 ± 0% | $1.99 \times 10^4$ ± 0% | 0 | 9 | |
| 15 | $Mg_{0.7}Fe_{0.3}SiO_3$ (p/g) | 57.3 ± 1% | 1.24 ± 0% | $4.56 \times 10^4$ ± 0% | 0 | 8 | |
| 16 | $Fe_2SiO_4$ (f/c) | na[h] | 0.82 ± 1% | $7.56 \times 10^4$ ± 1% | na[h] | na[h] | |
| 17 | $Mg_{0.8}Fe_{0.2}SiO_3$ (p/g) | 64.6 ± 1% | 1.13 ± 0% | $7.72 \times 10^4$ ± 0% | 0 | 7 | |
| 18 | $Mg_{1.72}Fe_{0.21}SiO_4$ (o/c) | 1.4 ± 130% | 0.39 ± 8% | $3.35 \times 10^5$ ± ± 0% | 0 | na[g] | |
| 19 | $Mg_{1.9}Fe_{0.1}SiO_4$ (o/c) | 3.0 ± 112% | 0.48 ± 12% | $6.67 \times 10^5$ ± 3% | 0 | 1 | |
| 20 | $Mg_2SiO_4$ (Ms/a) | 11.6 ± 37% | 1.12 ± 4% | $9.75 \times 10^5$ ± ± 5% | 15 | 1 | |
| 21 | $Mg_{2.4}SiO_{4.4}$ (Ms/a) | 11.5 ± 42% | 1.12 ± 5% | $1.08 \times 10^6$ ± 6% | 18 | 1 | |
| 22 | $Mg_{0.7}SiO_{2.7}$ (Ms/a) | 12.3 ± 22% | 1.21 ± 2% | $1.25 \times 10^6$ ± 3% | 0 | 1 | |
| 23 | $MgSiO_3$ (Ms/g) | 13.5 ± 68% | 1.11 ± 8% | $2.87 \times 10^6$ ± 10% | 0 | 0 | |
| 24 | $Mg_{1.5}SiO_{3.5}$ (Ms/a) | 98.1 ± 1% | 2.05 ± ± 0% | $4.03 \times 10^7$ ± 82% | 0 | 1 | |
| 25 | $SiO_2$ (Silica/a) | 108.5 ± 0% | 2.06 ± 0% | $1.61 \times 10^8$ ± 82% | 0 | 1 | |

[a]Substance names abbreviated as follows: m: magnetite, mw: magnesiowüstite, o: olivine, p: pyroxene, w: wüstite, f: fayalite, ms: magnesium silicate, h: hematite. [b]Substance phase as follows, a: amorphous, g: glassy, c: crystalline, ?: unknown. [c]Average and standard deviation of model results for April–May and $0.2 < P < 0.01$ hPa. [d]Based on SOFIE observations at 0.2–0.02 hPa during April–May 2011 at ~70°S. [e]Based on SOFIE observations of smoke contained in PMC particles as in Hervig et al. (2012). [f]The influx of ablated iron determined for the 10 most likely smoke compositions in this work (see text for detail). The uncertainty in Fe influx is ~7% for all compositions. [g]Composition not considered in Hervig et al. (2012). [h]Refractive index not available for 330 nm wavelength.

105 km (~0.3 to 0.001 hPa) with a precision of ~10 ppbv at altitudes below ~85 km (Gordley et al., 2009; Smith et al., 2013). Below ~55 km a Whole Atmosphere Community Climate Model (WACCM) $O_3$ climatology was used. Because $O_3$ interference is on par with the smoke signal below 53 km ($P \gtrsim 0.3$ hPa) at 330 and 867 nm (Figures 1c and 1d), these extinctions were only used at higher altitudes in this work.

## 3. Meteoric Smoke Models

A three-dimensional global model of meteoric smoke was described by Bardeen et al. (2008), using a purely climatological atmosphere in the defined above WACCM. The present study used an adaptation of these smoke simulations within the specified dynamics WACCM version 4 model, which has a higher horizontal resolution (1.9° × 2.5°) (Marsh et al., 2013). The WACCM runs incorporated meteorological values of winds and temperature below 50 km from the Goddard Earth Observing System 5 (GEOS-5) analyses (Lamarque et al., 2012). Meteoroid ablation products are introduced in the model as smoke particles with 0.2 nm radius (i.e., essentially molecular clusters), which then undergo coagulation and transport. The model reports vertical profiles of smoke concentration versus radius, which can be used to determine smoke properties such as volume density ($V$) or extinction. This version, known here as WACCM-1 (run for 2007–2012), was used in a recent investigation of SOFIE smoke observations by Hervig et al. (2017). WACCM-1 was shared with the University of Leeds, where a variety of enhancements have been implemented (known here as WACCM-2). WACCM-2 includes the detailed gas phase chemistry of meteoric metals as described in Plane et al. (2015). It has also been modified to include the interactions between MSPs and various trace gases (Frankland et al., 2015; James et al., 2017). WACCM-2 was run for 2007–2014, using meteorological fields from the Modern-Era Retrospective Analysis for Research and Applications

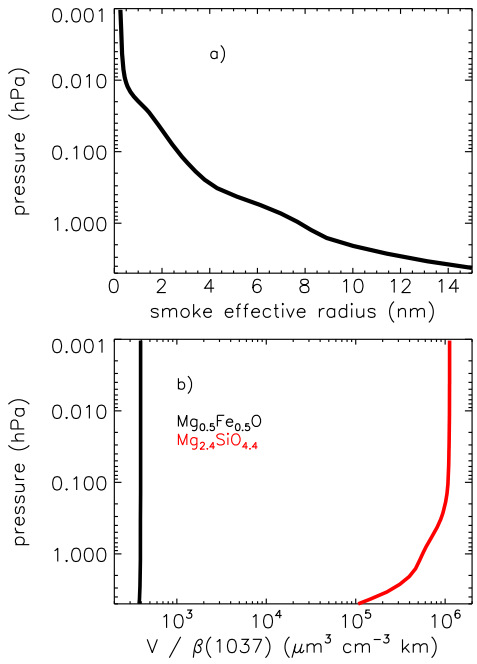


**Figure 2.** Average profiles based on model smoke size distributions near ~70°S latitude during April—May 2011. (a) Smoke effective radius ($r_e = \sum r^3 / \sum r^2$, where the summation is over radii in the size distribution). (b) The ratio of smoke volume density over 1,037 nm extinction, for two smoke compositions.

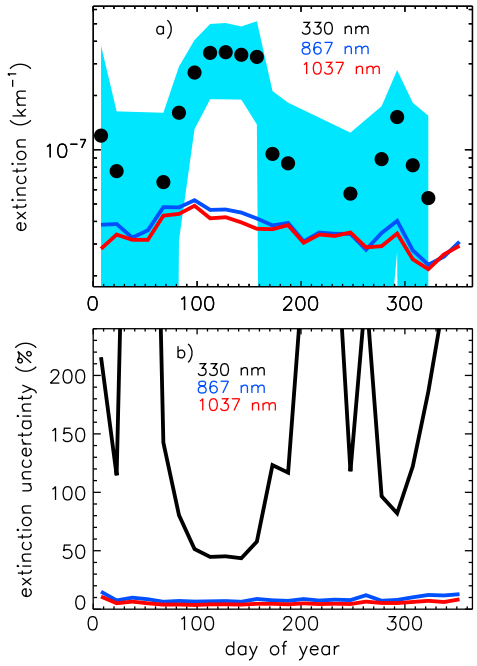


**Figure 3.** Time series at 0.1 hPa pressure (~60 km) as 15 day averages of SOFIE results during 2011 near ~70°S latitude. (a) Measured smoke extinction at three wavelengths as indicated. The light blue shading indicates the 330 nm extinction uncertainties. (b) The extinction uncertainties for three wavelengths. Note that the 330 nm uncertainties can exceed the vertical scale.

reanalysis (Rienecker et al., 2011) (which is based on GEOS-5). Using these two WACCM versions provides confidence in the simulations and allows an assessment of how the model changes have affected the resulting smoke.

Meteoric smoke composition is constrained below by comparing the multiwavelength extinction measurements to predictions for a variety of compounds as listed in Table 1. The list of smoke compositions considered here was motivated by previous work (e.g., Hervig et al., 2012; Saunders & Plane, 2006), but ultimately limited to the refractive indices available for the SOFIE wavelengths (Henning et al., 1999; Jaeger et al., 2002). Most of the compounds considered are a combination of iron, silica, and magnesium, which represent the major metallic species found in meteoroids (Carrillo-Sánchez et al., 2016; Plane, 2012).

Smoke extinctions were simulated for spherical particles using modeled particle size distributions versus height (Bardeen et al., 2008). Most compositions do not scatter but rather absorb radiation at SOFIE wavelengths, for particle radii indicated by the MSP models ($r < 10$ nm; see Figure 2a). This is due to a large imaginary refractive index, and indeed is the reason that smoke can be detected by SOFIE. Because aerosol absorption is proportional to particle volume, the measured smoke extinctions are directly proportional to $V$. The relationship between $\beta$ and $V$ is therefore independent of particle size and concentration, and determined solely by the refractive index (i.e., composition), for all but the most weakly absorbing compounds. This is demonstrated in Figure 2b, where example results are shown for a strong ($Mg_{0.5}Fe_{0.5}O$) and weak ($Mg_2SiO_4$) absorber (see also Table 1). Note that $V/\beta(1037)$ for the weak absorber decreases for $P \gtrsim 0.1$ hPa (below ~60 km), which is due to an increase in particle size (and therefore scattering efficiency). This moderate dependence on particle size only appears for the weakest absorbers (numbers 18–25 in Table 1). For the strongly absorbing smoke candidates, the wavelength dependence of extinction depends solely on refractive index. Modeled extinction ratios are listed in Table 1, as the average and standard deviation for April–May at 0.2–0.01 hPa. These results further illustrate that the wavelength dependence of extinction is independent of particle size for the strong absorbers, as the extinction ratios have miniscule standard deviations for most compositions. The weakest absorbers can have large standard deviations in extinction ratio, which is due to the effect of scattering efficiency changing with particle size. These characteristics are considered below when comparing the model results with SOFIE in order to constrain smoke composition.

## 4. Meteoric Smoke Composition

The composition of meteoric smoke was constrained by comparing model results with multiwavelength extinctions measured during 2011 near ~70°S latitude. The annual cycle in smoke is due to transport by the global meridional circulation, with the greatest smoke volume density in fall/winter and a minimum in summer (Hervig et al., 2017; Megner et al., 2008). An example of the annual cycle in observed extinctions is shown in Figure 3 for 0.1 hPa. The annual cycle in the 867 and 1,037 nm wavelength extinctions is similar and consistent with previously published results (e.g., Hervig et al., 2017). Uncertainties in the

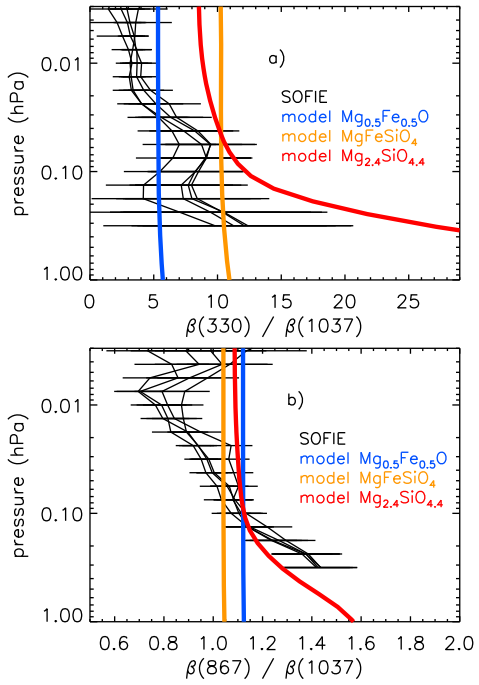


**Figure 4.** Vertical profiles of the ratio of (a) 330/1,037 nm and (b) 867/1,037 nm smoke extinction. SOFIE results are 15 day averages during April–May 2011 (four profiles) near 70°S. The horizontal lines indicate the SOFIE uncertainties. Model results are shown for the same time and location, considering three smoke compositions as indicated.

330 nm extinctions are very high (>100%), except during April–May when they decrease to ~50% (Figures 3a and 3b). The lower uncertainties during fall/winter are due primarily to the increase in smoke, and also to seasonal variations in ozone. In any case, errors in the 330 nm extinctions preclude their use in examining seasonal variations in smoke. Considering the errors in measured 330 nm extinction, the analysis of composition, which requires all three wavelengths, was restricted to April–May when the 330 nm uncertainties are lowest. Using the SOFIE results as 15 day averages further reduces random uncertainties, which is important primarily for the 330 nm extinctions.

Measured extinction ratios versus height are compared to model results in Figure 4. The 330/1,037 nm extinction ratio varies in height; however, these variations are not interpreted physically as they are within the measurement uncertainties. The 867/1,037 nm extinction ratio (Figure 4b) increases from ~0.8 near 0.01 hPa to ~1.2 near 0.2 hPa. This change is slightly within the measurement uncertainty and thus could be indicative of changes in smoke over height. SOFIE is compared to modeled extinction ratios in Figure 4, for two strongly absorbing compounds ($Mg_{0.5}Fe_{0.5}O$ and $MgFeSiO_4$) and a weak absorber ($Mg_2SiO_4$). The extinction ratios are constant in height for the strong absorbers, due to the prevalence of absorption as discussed in section 3. Note that for the weak absorber, the extinction ratios increase for $P > 0.1$ hPa (Figure 4). This is due to a corresponding increase in particle size (see Figure 2a), which results in increased scattering efficiency. Note, however, that the weakly absorbing compounds (i.e., high $V/\beta$; see Table 1) are unlikely to be major constituents, because their presence would imply that there is >1,000 times more smoke in the mesosphere than is currently thought. It is tempting to interpret the observed extinction ratios to indicate changing smoke composition with height. This analysis would be tenuous, however, because the uncertainties in 330 nm extinction are too large to asses such height dependence and because composition cannot be constrained with any confidence using only the 867 and 1,037 nm wavelengths.

As discussed above, the ability to constrain smoke composition is limited by the 330 nm extinction uncertainties, which are tolerably low (≲50%) only during April–May (Figure 3b), and for pressures from 0.2 to 0.02 hPa (Figure 1b). The probability distribution of measured extinction ratios for these heights and times is compared to model results in Figure 5a. The model values are based on smoke radii from WACCM-1 (Bardeen et al., 2008) and are as listed in Table 1 (see section 3 for details). Note that the modeled extinctions ratios are insensitive to particle size (with the exception of a few of the weakest absorbers, i.e., #18–23 in Table 1) and do not change when using the various other WACCM model runs. By definition, the extinction ratios are also insensitive to smoke concentration, as this cancels in the ratio. As stated above, the extinction ratios examined here are only sensitive to refractive index and thus composition. The SOFIE measurements are clearly consistent with certain smoke compositions but not others. The possibility that a model composition was consistent with SOFIE was quantified by computing the model-measurement separation, in terms of the two extinction ratios, $\beta(330)/\beta(1037)$ versus $\beta(867)/\beta(1037)$. If this separation was within the distance corresponding to 25% uncertainties for a given observation, then the model composition was considered to have been detected. The probability of detecting a given composition is simply the number of detections over the number of observations. The measured extinction ratio uncertainties were fixed to 25% (roughly the average in the 867/1,037 nm extinction ratios for April–May and $0.2 < P < 0.02$ hPa) to prevent instances where large measurement uncertainties erroneously permit many compositions to be detected. The model-measurement comparisons clearly permit multiple MSP compositions to be present simultaneously, due to the uncertainties and also the overlap in spectral signatures for various compositions (Table 1 and Figure 5). Detection probabilities for the compositions considered are quantified in Table 1 based on comparing the model to measurements as 15 day averages during April–May 2011 (~70°S latitude) and pressures from 0.2 to 0.02 hPa. Note that the detection probabilities in Table 1 (which consider model-measurement

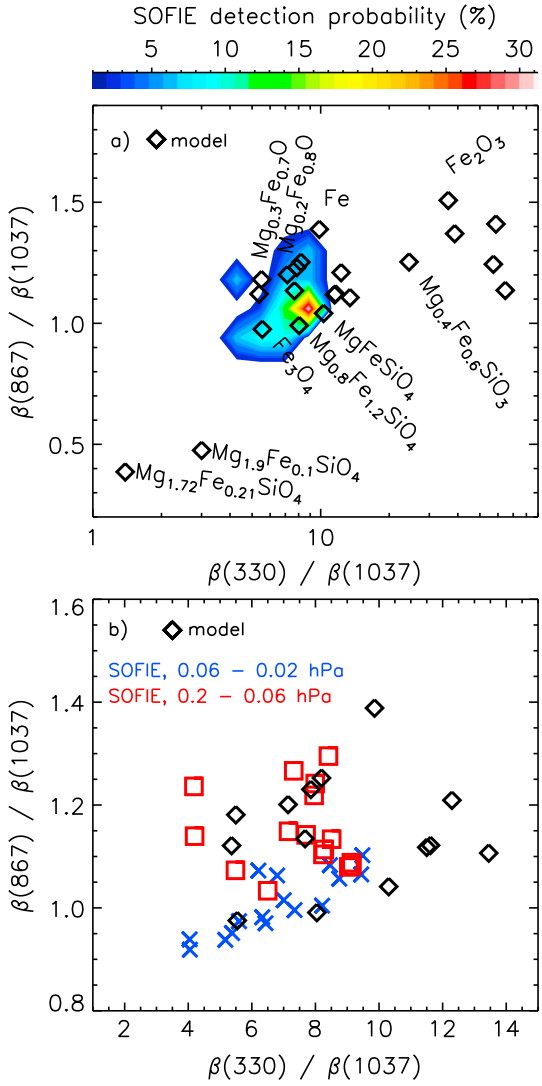


**Figure 5.** SOFIE extinction ratio measurements as 15 day averages during April–May 2011 (~70°S latitude), compared to model results for various smoke compositions. Only a few of the model points are labeled for visual clarity. More detail on the model results and the probability of detecting each composition can be found in Table 1. (a) SOFIE results shown as a probability distribution based on measurements from 0.2 to 0.02 hPa pressure. (b) SOFIE results shown as discrete points for either 0.2–0.06 hPa or 0.06–0.02 hPa. Note that the model points are not labeled, that the axes have different scales, and that observation density is inherently difficult to discern from the discrete points (i.e., due to overlap).

comparisons) are not comparable to the values in Figure 5a, which are simply the probability that a measurement occurred within a discrete interval. The most likely MSP compositions are magnetite ($Fe_3O_4$), wüstite, magnesiowüstite ($Mg_xFe_{1-x}O$, $x$ = 0–0.6), and iron-rich olivine ($Mg_{2x}Fe_{2-2x}SiO_4$, $x$ = 0.4–0.5). The results exclude smoke compositions of proxene, hematite, iron-poor olivine ($x$ = ~0.9), and silica. While magnesium silicates (#19 and 20) are permitted by the observations, it is argued that these compounds are unlikely to have been measured because of their extremely weak optical signatures.

It was shown above (Figure 4) that the measured extinction ratios vary in height. This variability is further examined in Figure 5b, where the model is compared to SOFIE points separated for different height regions (0.2–0.06 hPa and 0.06–0.02 hPa). While these results are not rigorously interpreted in terms of varying composition, they do impart a sense of the changing optical signatures in height. Note that the probability distribution in Figure 5a more clearly indicates the density of the observations, which cannot be discerned when showing individual data points (which overlap) as in Figure 5b.

In the model-measurement comparisons (i.e., Table 1 and Figure 5a), 12% of the SOFIE extinction ratios are not explained by the model compositions considered here. Some of these could be consistent with a model result if the uncertainties were increased. It is also reasonable to consider that smoke particles may be composed of a mixture of two or more substances. The optics of a mixed particle can be simulated using different approaches, such as concentric spheres or by using the refractive index of an effective medium mixture (these approaches give nearly identical results) (e.g., Hervig et al., 2012). The possibility of mixed particles was considered by combining varying amounts (10 to 90% by volume) of one substance with the other 24 compounds considered and computing the effective medium refractive index. The simulated extinction ratios were compared to SOFIE, and indeed, many of these mixtures are consistent with the observations. The problem with arbitrarily creating mixed smoke particles from the available composition candidates, however, is that the measurements can be explained by a seemingly infinite number of mixtures. Consideration of mixed smoke compositions is therefore postponed until guidance concerning plausible mixtures is available. It should be noted that when mixing a weak absorber (e.g., iron-poor olivine) with a strong absorber (e.g., magnesiowüstite), the optical signature of the mixed particle can be nearly identical to that of the strong absorber (i.e., the weak material can be invisible). Thus, this study cannot confidently conclude that the detected smoke compositions do not also contain some amount of weakly absorbing material (e.g., within a mixture or as a coating). Addressing this issue will require additional measurements and new analysis techniques. Nevertheless, it can still be confidently stated that smoke particles are not composed of pure proxene, hematite, iron-poor olivine, magnesium silicate, or silica, because their wavelength dependence is not consistent with the measurements.

A previous analysis of SOFIE observations indicated that the ice particles comprising PMCs contain a small amount of meteoric smoke (Hervig et al., 2012). That study further demonstrated that MSPs contained in ice were most likely composed of carbon or magnesiowüstite ($Mg_xFe_{1-x}O$, $x$ = 0–0.6). The smoke composition detection probabilities from Hervig et al. (2012) are reproduced in Table 1 for comparison to the present results. The two approaches are broadly consistent, indicating that MSPs are composed of the strongly absorbing compounds (magnetite, wüstite, magnesiowüstite, and iron-rich olivine), and excluding the

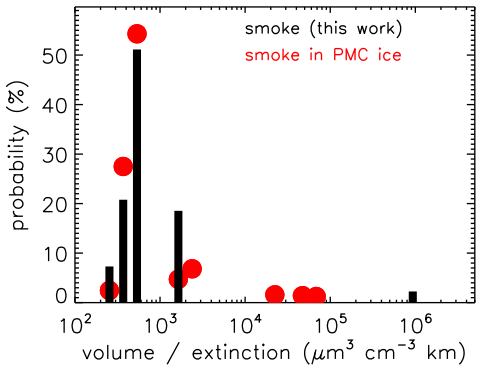


**Figure 6.** The probability that smoke $V/\beta$ lies within a discrete interval, for 30 intervals spaced logarithmically from 100 to $5 \times 10^6$ $\mu m^3$ $cm^{-3}$ km. The histograms are based on the composition detection probabilities as in Table 1. Results for smoke contained in PMC particles are from Hervig et al. (2012).

weak absorbers (proxene, iron-poor olivine, magnesium silicate, and silica). Based on the results in Table 1, it could be speculated that interactions with ice are favored by some compositions more than others. Such ideas are difficult to test, however, because meteoric smoke is drastically reduced during PMC season leading to greater measurement uncertainties and because SOFIE cannot measure ambient smoke when PMCs are present.

## 5. Smoke Volume Density

Information concerning smoke composition allows smoke volume density to be determined from the measured extinctions. The 1,037 nm extinction measurements are used for this purpose, since they have the smallest uncertainties and span the greatest altitude range. The conversion of SOFIE $\beta$ to $V$ was accomplished using model values of $V/\beta$ for the smoke compositions identified above. The detection probabilities for each smoke composition (Table 1) were used to examine the statistical distribution of $V/\beta$ (Figure 6). The results are examined in this way because many of the indicated compositions have similar values of $V/\beta$, and the current focus is only to characterize the best statistical representation of $V/\beta$. Results are shown for the present study, and also from measurements of smoke contained in PMC particles. Both approaches indicate a few instances of very high $V/\beta$ (i.e., $>10^4$ $\mu m^3$ $cm^{-3}$ km) but also show that the majority of smoke compositions have $V/\beta \lesssim 3 \times 10^3$ $\mu m^3$ $cm^{-3}$ km.

The average and standard deviation of the results can be misleading due to the few instances of very large values. It was argued above that the weakly absorbing compounds are unlikely to be major constituents (or to have been observed) because this would require that smoke volume densities of >1,000 times more than are currently thought to exist. For additional perspective, using $V/\beta$ of $10^4$–$10^6$ $\mu m^3$ $cm^{-3}$ km with SOFIE smoke extinctions would imply that smoke $V$ is 10–$10^3$ times greater than the volume density of sulfate aerosols in the upper stratosphere, and similar to values in polar stratospheric clouds. Neither of these scenarios seems likely, and the average $V/\beta$ was therefore determined for only $V/\beta < 10^4$ $\mu m^3$ $cm^{-3}$ km. The resulting average was $687 \pm 470$ $\mu m^3$ $cm^{-3}$ km ($695 \pm 645$ $\mu m^3$ $cm^{-3}$ km, for smoke in PMCs), and this value and uncertainty (as the standard deviation) were adopted below to estimate $V$ from the 1,037 nm extinctions. The approach of using an average value does not imply a certain composition (or mix of compositions). It rather acknowledges that different compositions could be present and is an attempt to capture a statistically reliable $V/\beta$ for deriving $V$ from the measurements. Note that the standard deviation in the mean $V/\beta$ is large (~68%), even when considering a truncated list of composition candidates. Additional uncertainties in the smoke $V$ determined form SOFIE will come from the extinction uncertainties (~15%; Figure 1b), so that total uncertainties in $V$ (when using the average $V/\beta$) are estimated to be ~70%.

## 6. Meteoric Influx

WACCM results indicate that when the meteoric influx is changed, the smoke volume density changes by nearly the same fractional amount at heights throughout the mesosphere. The dependence of $V$ on MI was determined by varying the MI in model runs with WACCM-1 (11, 44, and 110 t $d^{-1}$) and WACCM-2 (2, 8, and 11 t $d^{-1}$). The actual MI can then be estimated by comparing SOFIE observations of smoke $V$ with the modeled dependence of $V$ on MI. In this approach, we assume that SOFIE-model differences are due entirely to the model MI. This assumption was explored by examining the sensitivity of modeled $V$ to a variety of other factors including Brownian diffusion, the gravity wave parameterization that affects the vertical and horizontal winds, and the effect of smoke being incorporated in PMC particles. Changing any (or all) of these parameters in the model did not change the smoke $V$ appreciably (typically <~20%, not shown). Additionally, none of these parameters change $V$ by the same factor throughout the mesosphere, which is the case for adjusting MI. This is a relevant point because comparisons of SOFIE and WACCM $V$ (see below) indicate an offset that is reasonably constant in height, supporting the stance that SOFIE-model differences are attributable to MI. Note that the models describe only the ablated meteoric material (MI and therefore $V$) and that SOFIE $V$ also represent only the ablated material.

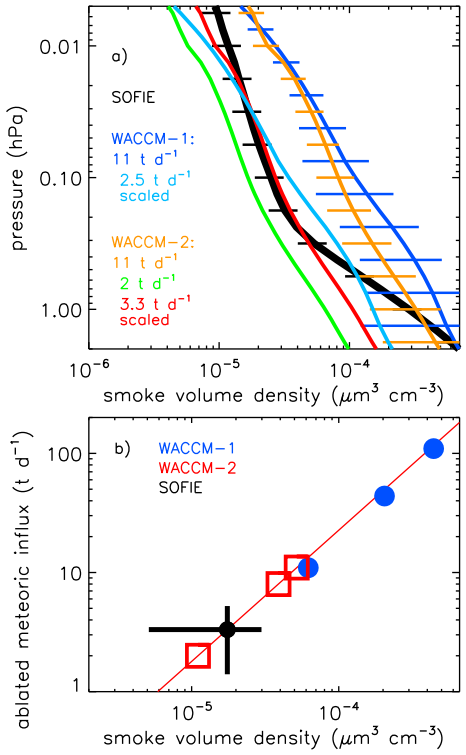


**Figure 7.** (a) Smoke $V$ profiles as averages for April–October 2011 near 70°S, from SOFIE and the models. WACCM-1 $V$ are shown for a run with 11 t d$^{-1}$, and also for scaling to a MI that matches SOFIE (2.5 t d$^{-1}$). WACCM-2 $V$ are shown for MI of 2 and 11 t d$^{-1}$, and also for scaling to match SOFIE (3.3 t d$^{-1}$). (b) Smoke $V'$ (i.e., averaged over 0.1–0.01 hPa) versus ablated MI for two WACCM versions. Also shown are a regression to the WACCM-2 results (red line), and the MI estimated using SOFIE $V'$ with the regression parameters, log(MI) = 5.76 + 1.10 log($V'$).

Smoke volume density profiles from SOFIE and the models are compared in Figure 7a, for averages during April–October 2011. Note that sulfate aerosols are ubiquitous for $P \gtrsim 5$ hPa. Furthermore, it was recently shown that a layer of neutralized $H_2SO_4$ mixed with meteoric smoke is present during autumn for $P \gtrsim 0.5$ hPa (Hervig et al., 2017). To ensure that the present analysis examines only meteoric smoke, the results only considered pressures <0.5 hPa to avoid possible contamination by $H_2SO_4$. Both versions of WACCM were run for MI = 11 t d$^{-1}$ and are in good agreement for pressures less than ~0.05 hPa, with small but increasing differences at greater pressures. These relatively small differences are primarily related to assimilating different meteorological analyses. It is clear that model $V$ for a MI of 11 t d$^{-1}$ are roughly four times greater than SOFIE and that reducing MI will bring the model into agreement with the observations (see model $V$ for 2 t d$^{-1}$ in Figure 7a).

The model results were used to estimate the ablated MI with SOFIE, using $V$ as averages for the middle mesosphere ($0.1 < P < 0.01$ hPa). This approach reduces some uncertainties that could arise due to vertical variations that are not present in both the model and measurements. The vertically averaged $V$ ($V'$) versus MI were fit using linear regression (WACCM-1 and WACCM-2 were used separately, and together), as illustrated in Figure 7b. For this purpose, the fit was performed on log($V'$) and log(MI), to account for a slight nonlinearity in the relationship. An estimate of MI was then obtained using the regression parameters with the SOFIE $V'$, averaged over the same times and heights as the model results. Using SOFIE with WACCM-1 indicates MI = 2.5 ± 1.4 t d$^{-1}$, and SOFIE with WACCM-2 gives MI = 3.3 ± 1.9 t d$^{-1}$. A regression was also performed to $V'$ versus MI using the WACCM-1 and WACCM-2 results together, giving MI = 3.2 ± 1.9 t d$^{-1}$. The stated uncertainties are due to errors in the SOFIE smoke volume densities and due to errors in the regression to model $V'$ versus MI. These terms were captured in a Monte Carlo analysis, with the final uncertainty (~58%) taken as the standard deviation of $10^6$ perturbations. It is evident that the height dependence of SOFIE $V$ is in slightly better agreement with WACCM-2 than WACCM-1 (Figure 7a). Additionally, the WACCM-2 MI (and thus $V$) values bracketed SOFIE, whereas WACCM-1 levels were much higher. Thus, the SOFIE-WACCM-2 comparisons have slightly greater confidence, and these results are adopted for the quoted MI from this work. Note that the SOFIE-WACCM MI estimates are for averages of April–October, 2011 and that using a subset of these months does not appreciably change the MI results. It was mentioned above that the present study cannot exclude the possibility that some weakly absorbing material is mixed with the indicated smoke compositions. If this were true, then the SOFIE $V$, and therefore MI, would be underestimates. Because there is no indication that such mixtures exist, however, we refrain from further consideration of this issue. Finally, while the $V$ and therefore MI estimates depend on the smoke composition results from this study (section 4), the stated MI are very close to estimates based on the compositions indicated for smoke in PMC particles (Hervig et al., 2012).

The present results can be used to characterize the influx of individual elements and also to estimate the total meteoric influx (ablated plus surviving material). Since the top 10 most likely compositions all contain iron, the ablated Fe influx (MI(Fe)) was examined first. For this purpose $V'$ was calculated from the SOFIE extinctions, using the value of $V/\beta$ (Table 1) for a specific smoke composition. MI was determined from $V'$ using the regression parameters for WACCM-2 (Figure 7b), and MI(Fe) is simply MI multiplied by the weight fraction of Fe in the compound. This approach recognizes that MI varies when using the $V/\beta$ for an individual composition, and also that the MSP can contain other elements. Note that for certain compositions (#2, 8, and 10 in Table 1) a small additional enhancement (11%) in MI(Fe) is required because the Mg/Fe ratio exceeds the Mg/Fe elemental ablation ratio of 0.9 (Carrillo-Sánchez et al., 2016). This enhancement represents the

additional ablation required to provide the necessary Mg in these compounds. Ablated Fe influx values determined as above are listed in Table 1 for the top 10 compositions, where MI(Fe) ranges from 0.8 to 3.6 t $d^{-1}$. The individual MI(Fe) estimates have relatively low uncertainties (~7%), which are due to measurement errors (reduced in averaging) and errors in the model regression. Nevertheless, MI(Fe) varies greatly for the different compositions, due to changing $V/\beta$ and Fe abundance. Because it is difficult to separate experimental uncertainties from physical variability in MI(Fe), the probability weighted average is taken as the most representative value, MI(Fe) = 1.8 ± 0.9 t $d^{-1}$. The uncertainty (~50%) is a combination of the MI(Fe) errors and the standard deviation of the 10 estimates in Table 1. A similar analysis as above was conducted to characterize the ablated magnesium influx, and the seven most likely compositions that contain Mg give a weighted mean MI(Mg) = 0.5 ± 0.5 t $d^{-1}$. The Mg result has greater uncertainty because fewer compounds contained Mg and because it is typically a minor constituent.

Carrillo-Sánchez et al. (2016) determined meteoric influx by constraining models with observations of atomic metals in the mesosphere and the accumulation rates of cosmic spherules at South Pole. Their results indicate an ablated Fe influx of 2.6 t $d^{-1}$, which is ~30% higher than the present estimate of 1.8 t $d^{-1}$. Carrillo-Sánchez et al. report a total meteoric influx (TMI) of 43.3 ± 14 t $d^{-1}$, but that only 7.9 t $d^{-1}$ (18%) of this material is ablated and therefore a source for smoke in the middle atmosphere. Their results allow a straightforward estimate of TMI from the present study, by multiplying the SOFIE-WACCM MI(Fe) by the ratio of TMI/MI(Fe) (43.3 t $d^{-1}$/2.6 t $d^{-1}$) from Carrillo-Sánchez et al. For this approach the average MI(Fe) from the present study implies a total meteoric influx of 30 ± 18 t $d^{-1}$. While this estimate has large uncertainties (~58%, determined as above) and is not independent of Carrillo-Sánchez et al. (2016), it should prove useful in refining the currently broad range in TMI estimates (5 to 270 t $d^{-1}$) (Gardner et al., 2014; Plane, 2012).

## 7. Summary

The composition of meteoric smoke particles in the mesosphere was constrained by comparing SOFIE observations at three wavelengths with model results. The observations are consistent with smoke compositions of magnetite, wüstite, magnesiowüstite, or iron-rich olivine. The results furthermore indicate that smoke is not composed purely of proxene, hematite, iron-poor olivine, magnesium silicate, or silica (which are weakly absorbing). Note that these weakly absorbing compositions could be present in a particle of mixed components (e.g., as a coating on a strong absorber) and not be detected by the present methods. Confirming this possibility, however, will require new and different observations. The constraints on smoke composition are generally consistent with a previous analysis of meteoric smoke detected in PMC particles. The observations may indicate height variations in smoke composition; however, the ability to explain these variations may be outside the capability of the measurements. Smoke volume densities were determined from the SOFIE extinctions using modeled optics based on the compositions identified here. The ablated fraction of meteoric influx was then estimated by comparing observed smoke volume with modeled volume versus meteoric influx. The results indicate an ablated meteoric influx of 3.3 ± 1.9 t $d^{-1}$, which is considered to represent the sum of Fe, Mg, and possibly Si. More specifically, the ablated influx was estimated for individual elements, indicating 1.8 ± 0.9 t $d^{-1}$ for Fe and 0.5 ± 0.5 t $d^{-1}$ for Mg. Finally, the global total meteoric influx was estimated to be 30 ± 18 t $d^{-1}$, given a recent description of the influx and ablation of individual meteoric species.

**Acknowledgments**
This work was funded in part by the AIM mission through NASA's Small Explorers Program under contract NAS5-03132. The modeling work at the University of Leeds was supported by the European Research Council (project 291332-CODITA). SOFIE data are available online at sofie.gats-inc.com. The updated SOFIE extinctions used in this study are available by contacting Mark Hervig (mark@gats-inc.com). WACCM-1 model results are available by contacting Charles Bardeen (bardeenc@ucar.edu). The WACCM2 data sets generated for this work have been archived at the Leeds University PETAL (PetaByte Environmental Tape Archive and Library) www.see.leeds.ac.uk/business-and-consultation/facilities/petabyte-environmental-tape-archive-and-library-petal.

## References

Bardeen, C. G., Toon, O. B., Jensen, E. J., Marsh, D. R., & Harvey, V. L. (2008). Numerical simulations of the three-dimensional distribution of meteoric dust in the mesosphere and upper stratosphere. *Journal of Geophysical Research*, *113*, D17202. https://doi.org/10.1029/2007JD009515

Bohren, C. F., & Olivero, J. J. (1984). Evidence for haematite particles at 60 km altitude. *Nature*, *310*(5974), 216–218. https://doi.org/10.1038/310216a0

Carrillo-Sánchez, J. D., Nesvorný, D., Pokorný, P., Janches, D., & Plane, J. M. C. (2016). Sources of cosmic dust in the Earth's atmosphere. *Geophysical Research Letters*, *43*, 11,979–11,986. https://doi.org/10.1002/2016GL071697

Frankland, V. L., James, A. D., Feng, W., & Plane, J. M. C. (2015). The uptake of $HNO_3$ on meteoric smoke analogues. *Journal of Atmospheric and Solar-Terrestrial Physics*, *127*, 150–160. https://doi.org/10.1016/j.jastp.2015.01.010

Gardner, C. S., Liu, A. Z., Marsh, D. R., Feng, W., & Plane, J. M. C. (2014). Inferring the global cosmic dust influx to the Earth's atmosphere from lidar observations of the vertical flux of mesospheric Na. *Journal of Geophysical Research: Space Physics*, *119*, 7870–7879. https://doi.org/10.1002/2014JA020383

Gordley, L. L., Hervig, M. E., Fish, C., Russell, J. M. III, Bailey, S., Cook, J., … Kemp, J. (2009). The Solar Occultation For Ice Experiment (SOFIE). *Journal of Atmospheric and Solar: Terrestrial Physics*, *71*, 300–315. https://doi.org/10.1016/j.jastp.2008.07.012

Havnes, O., & Næsheim, L. I. (2007). On the secondary charging effects and structure of mesospheric dust particles impacting on rocket probes. *Annales de Geophysique*, *25*, 623–637. https://doi.org/10.5194/angeo-25-623-2007

Hedin, J., Gumbel, J., Waldenmarsson, T., & Glovane, F. (2007). The aerodynamics of the MAGIC meteoric smoke sampler. *Advances in Space Research*, *40*, 818–824. https://doi.org/10.1016/j.ars.2007.06.046

Henning, T., Il'in, V. B., Krivova, N. A., Michel, B., & Voshchinnikov, N. V. (1999). WWW database of optical constants for astronomy. *Astronomy and Astrophysics Supplement*, *136*(2), 405–406. https://doi.org/10.1051/aas:1999222

Hervig, M. E., Bardeen, C. G., Siskind, D. E., Mills, M. J., & Stockwell, R. (2017). Meteoric smoke and $H_2SO_4$ aerosols in the upper stratosphere and mesosphere, *Geophysical Research Letters*, *44*, 1150–1157. https://doi.org/10.1002/2016GL072049

Hervig, M. E., Deaver, L. E., Bardeen, C. G., Russell, J. M., Bailey, S. M., & Gordley, L. L. (2012). The content and composition of meteoric smoke in mesospheric ice particles from SOFIE observations. *Journal of Atmospheric and Solar: Terrestrial Physics*, *84-85*, 1–6. https://doi.org/10.1016/j.jastp.2012.04.005

Hervig, M. E., Gordley, L. L., Deaver, L. E., Siskind, D. E., Stevens, M. H., Russell, J. M. III, … Bardeen, C. G. (2009). First satellite observations of meteoric smoke in the middle atmosphere. *Geophysical Research Letters*, *36*, L18802. https://doi.org/10.1029/2009GL039737

Jaeger, C., Il'in, V. B., Henning, T., Mutschke, H., Fabian, D., Semenov, D. A., & Voshchinnikov, N. V. (2002). A database of optical constants of cosmic dust analogs. *Journal of Quantitative Spectroscopy and Radiation Transfer*, *79-80*, 765–774. https://doi.org/10.1016/S0022-4073(02)00301-1

James, A. D., Moon, D. R., Feng, W., Lakey, P. S. J., Frankland, V. L., Heard, D. E., & Plane, J. M. C. (2017). The uptake of $HO_2$ on meteoric smoke analogues. *Journal of Geophysical Research: Atmospheres*, *122*, 554–565. https://doi.org/10.1002/2016JD025882

Janches, D., Palo, S., Lau, E. M., Avery, S. K., Avery, J. P., de la Peña, S., & Makarov, N. A. (2004). Diurnal and seasonal variability of the meteor flux at the South Pole measured with radars. *Geophysical Research Letters*, *31*, L20807. https://doi.org/10.1029/2004GL021104

Klekociuk, A. R., Brown, P. G., Pack, D. W., ReVelle, D. O., Edwards, W. N., Spalding, R. E., … Zagari, J. (2005). Meteoritic dust from the atmospheric disintegration of a large meteoroid. *Nature*, *436*, 1132–1135. https://doi.org/10.1038/nature03881

Lamarque, J.-F., Emmons, L. K., Hess, P. G., Kinnison, D. E., Tilmes, S., Vitt, F., … Tyndall, G. K. (2012). CAM-chem: Description and evaluation of interactive atmospheric chemistry in the Community Earth System Model. *Geoscientific Model Development*, *5*, 369–411. https://doi.org/10.5194/gmd-5-369-2012

Marsh, D. R., Janches, D., Feng, W., & Plane, J. M. C. (2013). A global model of meteoric sodium. *Journal of Geophysical Research: Atmospheres*, *118*, 11,442–11,452. https://doi.org/10.1002/jgrd.50870

Marsh, D. R., Mills, M. J., Kinnison, D. E., Lamarque, J. F., Calvo, N., & Polvani, L. M. (2013). Climate change from 1850 to 2005 simulated in CESM1(WACCM). *Journal of Climate*, *26*(19), 7372–7391. https://doi.org/10.1175/JCLI-D-12-00558.1

Marshall, B. T., Deaver, L. E., Thompson, R. E., Gordley, L. L., McHugh, M. J., Hervig, M. E., & Russell, J. M. III (2010). Retrieval of temperature and pressure using broadband solar occultation: SOFIE approach and results. *Atmospheric Measurement Techniques Discussions*, *3*, 5743–5794. https://doi.org/10.5194/amtd-3-5743-2010

Megner, L., Siskind, D. E., Rapp, M., & Gumbel, J. (2008). Global and temporal distribution of meteoric smoke; a 2D simulation study. *Journal of Geophysical Research*, *113*, D03202. https://doi.org/10.1029/2007JD009054

Murphy, D. M., Thompson, D. S., & Mahoney, M. J. (1998). In situ measurements of organics, meteoric material, mercury, and other elements in aerosols at 5 to 19 kilometers. *Science*, *282*(5394), 1664–1669. https://doi.org/10.1126/science.282.5394.1664

Plane, J. M. C. (2012). Cosmic dust in the Earth's atmosphere. *Chemical Society Reviews*, *41*, 6507–6518. https://doi.org/10.1039/c2cs35132c

Plane, J. M. C., Feng, W., & Dawkins, E. C. M. (2015). The mesosphere and metals: Chemistry and changes. *Chemical Reviews*, *115*(10), 4497–4541. https://doi.org/10.1021/cr500501m

Rapp, M., Plane, J. M. C., Strelnikov, B., Stober, G., Ernst, S., Hedin, J., … Hoppe, U.-P. (2012). In situ observations of meteor smoke particles (MSP) during the Geminids 2010: Constraints on MSP size, work function and composition. *Annales Geophysicae*, *30*, 1661–1673. https://doi.org/10.5194/angeo-30-1661-2012

Rienecker, M., Suarez, M. J., Gelaro, R., Todling, R., Bacmeister, J., Liu, E., … Woollen, J. (2011). MERRA: NASA's Modern-Era Retrospective analysis for Research and Applications. *Journal of Climate*, *24*, 3624–3648. https://doi.org/10.1175/JCLI-D-11-00015.1

Rotundi, A., & Rietmeijer, F. J. M. (2008). Carbon in meteoroids: Wild 2 dust analyses, IDPs and cometary dust analogues. *Earth, Moon and Planets*, *102*, 473–483. https://doi.org/10.1007/s11038-007-9218-7

Russell, J. M. III, Bailey, S. M., Gordley, L. L., Rusch, D. W., Horányi, M., Hervig, M. E., … Merkel, A. W. (2009). Aeronomy of Ice in the Mesosphere (AIM): Overview and early science results. *Journal of Atmospheric and Solar: Terrestrial Physics*, *71*, 289–299. https://doi.org/10.1016/j.jastp.2008.08.011

Saunders, R. W., & Plane, J. M. (2011). A photo-chemical method for the production of olivine nanoparticles as cosmic dust analogues. *Icarus*, *212*, 373–382. https://doi.org/10.1016/j.icarus.2010.12.019

Saunders, R. W., & Plane, J. M. C. (2006). A laboratory study of meteor smoke analogues: Composition, optical properties and growth kinetics. *Journal of Atmospheric and Solar: Terrestrial Physics*, *68*, 2182–2202. https://doi.org/10.1016/j.jastp.2006.09.006

Singer, W., von Zahn, U., & Weiß, J. (2004). Diurnal and annual variations of meteor rates at the arctic circle. *Atmospheric Chemistry and Physics*, *4*, 1355–1363. https://doi.org/10.5194/acp-4-1355-2004

Smith, A. K., Harvey, V. L., Mlynczak, M. G., Funke, B., Garcia-Comas, M., Hervig, M., … Walker, K. A. (2013). Satellite observations of ozone in the upper atmosphere. *Journal of Geophysical Research: Atmospheres*, *118*, 5803–5821. https://doi.org/10.1002/jgrd.50445

Summers, M. E., & Siskind, D. E. (1999). Surface recombination of O and $H_2$ on meteoric dust as a source of mesospheric water vapor. *Geophysical Research Letters*, *26*(13), 1837–1840. https://doi.org/10.1029/1999GL900430

Taylor, S., Lever, J. H., & Harvey, R. P. (1998). Accretion rate of cosmic spherules measured at the south pole. *Nature*, *392*(6679), 899–903. https://doi.org/10.1038/31894

Vondrak, T., Plane, J. M. C., Broadley, S., & Janches, D. (2008). A chemical model of meteoric ablation. *Atmospheric Chemistry and Physics*, *8*, 7015–7031. https://doi.org/10.5194/acp-8-7015-2008